Theoretical Insight into the Redox-switchable Activity of Group 4 Metal Complexes for the Ring-Opening Polymerization of ε-Caprolactone

Journal:	*Inorganic Chemistry Frontiers*
Manuscript ID	QI-RES-11-2019-001466.R1
Article Type:	Research Article
Date Submitted by the Author:	01-Jan-2020
Complete List of Authors:	Xu, Xiaowei; Dalian University of Technology, School of Petroleum and Chemical Engineering Luo, Gen; Dalian University of Technology, Hou, Zhaomin; RIKEN Institute, Organometallic Chemistry Laboratory Diaconescu, Paula; UCLA, Chemistry and Biochemistry Luo, Yi; Dalian University of Technology, School of Chemcial Engineering

SCHOLARONE™
Manuscripts

ARTICLE

Theoretical Insight into the Redox-switchable Activity of Group 4 Metal Complexes for the Ring-Opening Polymerization of ε‑Caprolactone

Xiaowei Xu,[a] Gen Luo,*,[a] Zhaomin Hou,[b] Paula L. Diaconescu,*,[c] and Yi Luo*,[a]

Redox-switchable polymerization has drawn increasing attention, in particular for the ring-opening polymerization (ROP) of biomass-derived monomers. However, an understanding of how the switch determines the observed changes is still limited. In this study, DFT calculations were employed to understand the redox-switchable ROP mechanism of ε-caprolactone catalyzed by group 4 metal complexes bearing [OSSO]-type ferrocene ligands. Our results suggest that two oxidized forms show higher reactivity because of the higher Lewis acidity of their catalytic metal centers in comparison with that of the corresponding reduced states. In one case, however, a lower activity of the oxidized species was observed that is likely due to the increased stability of the substrate-catalyst intermediate leading to a high activation barrier. In addition, other analogous metal complexes were computationally modelled by changing the metal center or modifying the ancillary ligand with different bridging-heteroatoms, and the results provide useful information on the development of new redox-switchable polymerization catalysts.

Introduction

Polyesters are attractive materials due to their biodegradability and biocompatibility, and have been applied in the packaging or textile industry and biomedicine.[1] Therefore, the development of efficient strategies for the synthesis of such polymers is of great significance. In this context, the ring-opening polymerization (ROP) of cyclic esters catalyzed by single-site metal alkoxides is an efficient approach.[2] In particular, the redox-switchable ROP of cyclic esters has drawn an increasing attention in the last decade since it can regulate the (co)polymerization process and thus the resulting polymer microstructure.[3] In 2006, Long and Gibson first applied the redox-switchable strategy to the ROP of *rac*-lactide (LA) catalyzed by a titanium bis(iminophenoxide)(salen) complex bearing two ferrocenyl (Fc) units via altering the oxidation state of the ferrocene iron center.[4] Since then, several catalysts have been developed by either modulating the oxidation state of the central metal[5] or that of the supporting ligand.[6] For example, Byers and coworkers demonstrated that Fe(I) bis(imino)pyridine complexes were superior catalysts compared

to Fe(II)/Fe(III) analogues for the ROP of ε-caprolactone (CL).[5a] They further computationally investigated the role of the alkoxide initiator and the electronic structures of these redox-active iron species.[7] Their results suggested that the coordination of the lactone monomer is a key factor accounting for the reactivity trend. The redox non-innocence of the bis(imino)pyridine ligand allows access to a masked low-coordinate monoalkoxide Fe(II) center, which facilitates binding considerably relative to a similar bisalkoxide Fe(II) complex.
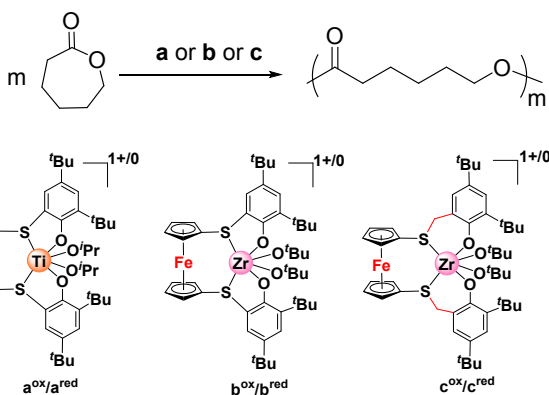
Furthermore, Diaconescu and co-workers[6b] demonstrated that an aluminum complex bearing an [OSSO]-type bis(phenolato) ferrocene ligand, (thiolfan*)Al(O^{t}Bu) (thiolfan* = 1,1'-di(2,4-di-*tert*-butyl-6-thiophenoxy)ferrocene), could catalyze CL/LA (co)polymerization. DFT calculations in that work suggested that the coordination of the carbonyl group of the pre-enchained monomer unit accounted for the propagation rate of such (co)polymerizations. In addition, a series of titanium and zirconium alkoxide complexes bearing similar ferrocene ligands, (thiolfan*)Ti(O^{i}Pr)$_2$, (thiolfan*)Zr(O^{t}Bu)$_2$, and (thiolfan)Zr(O^{t}Bu)$_2$ (thiolfan = (1,1'-di(2,4-di-*tert*-butyl-6-thiomethylenephenol)ferrocene), Table 1) were used for CL polymerization.[6a,f] As shown in Table 1, although the three couples of group 4 metal complexes ($\mathbf{a^{ox}}$/$\mathbf{a^{red}}$, $\mathbf{b^{ox}}$/$\mathbf{b^{red}}$, and $\mathbf{c^{ox}}$/$\mathbf{c^{red}}$) have a similar ancillary ligand framework, their oxidized and reduced forms demonstrated significantly diverse redox-switchable performance in CL polymerization. For instance, the oxidized forms $\mathbf{a^{ox}}$ and $\mathbf{c^{ox}}$ showed a higher activity toward CL polymerization compared with the corresponding reduced forms, $\mathbf{a^{red}}$ and $\mathbf{c^{red}}$. However, the $\mathbf{b}$ system showed a reverse redox-switchable behavior (Table 1).

[a.] State Key Laboratory of Fine Chemicals, School of Chemical Engineering, Dalian University of Technology, Dalian 116024, China. E-mail: luogen@dlut.edu.cn, luoyi@dlut.edu.cn
[b.] Organometallic Chemistry Laboratory, RIKEN Cluster for Pioneering Research, and Advanced Catalysis Research Group, RIKEN Center for Sustainable Resource Science, 2-1 Hirosawa, Wako, Saitama 351-0198, Japan.
[c.] Department of Chemistry and Biochemistry, University of California, Los Angeles, 607 Charles E. Young Drive East, Los Angeles, California 90095, United States. Email: pld@chem.ucla.edu

Table 1. Group 4 metal catalysts bearing [OSSO]-type bis(phenolato) ferrocene-based ligands for ε-caprolactone (CL) polymerization.[6a,6f]

entry[a]	compound[a]	Temp(°C)	Time (h)	Conv.(%)
1	a[ox]	100	4	48
2	a[red]	100	2	<5
3	b[ox]	50	20	84
4	b[red]	50	8	89
5	c[ox]	100	1.5	97
6	c[red]	100	1.5	52

[a] The right superscripts "ox" and "red" denote oxidized and reduced states, respectively.

These intriguing reactions indicate that the redox-switchable activity of such catalysts is strongly dependent on their supporting ligands and catalytic metal centers and, therefore, are an appropriate choice to study computationally.[8,9] The elucidation of the origin of the redox- switchable performance is not only of interest but also of importance for the further development of redox-switchable polymerization catalysts. In the present work, the mechanism of redox-switchable ROP of CL catalyzed by **a**, **b**, **c** (Table 1) is studied by DFT calculations. In addition, some potential group 4 metal analogues with a high performance for the redox-switchable ROP of CL are proposed on the basis of computational studies.

Computational details

The B3PW91 functional[10] corrected with the empirical dispersion term (known as Grimme-D3 with the zero-damping scheme)[11] was used for geometrical optimizations and subsequent frequency calculations without any symmetry or geometrical constraints. This functional has been successfully applied for metal complexes.[12] In these calculations, the 6-31G(d) basis set[13] was used for non-metallic atoms, while for Fe, Ti, Zr, and Hf, the effective core potentials (ECPs) of Hay and Wadt with a double-ζ valence basis set (LanL2DZ) were used.[14] Such basis sets are referred to as BSI. To obtain accurate energies, single-point energy calculations were performed for the optimized geometries at the level of M06[15]/BSII together with the CPCM model[16] (in benzene solution) to consider the solvation effect. In the BSII, the Stuttgart/Dresden ECP[17] and associated basis sets were used for metal atoms, and the 6-311G(d,p) was used for the remaining atoms. The right-superscripts "ox" and "red" of a given label (e.g., **a**[ox] or **a**[red])

denote the oxidized or reduced forms of the corresponding complex, respectively. The profiles of free energy in solution reported in this study were obtained at the M06/BSII (CPCM, benzene)//B3PW91-D3/BSI level, including the free energy correction taken from gas-phase frequency calculations. The corresponding relative enthalpies (ΔH, kcal mol^{-1}) are also provided for the estimation of entropy effects. All calculations were carried out using the Gaussian 16 program package,[18] and the spin-unrestricted manner was applied. For the sake of computational efficiency, the O^{t}Bu and O^{i}Pr groups were replaced by OMe groups. The computational model adopted here was successfully applied for similar systems in previous studies.[6b,c] The three-dimensional images of the optimized structures were prepared using CYLview.[19]

Results and discussion

Comparison of the active species

Before discussing the redox-switchable mechanism, the geometric and electronic characteristics of the oxidized and reduced species of **a**, **b**, and **c** were analysed. The computational results show that the doublet and singlet are the most stable states of the oxidized and reduced species, respectively, for each of the three cases. As shown in Fig. 1, each oxidized species has a similar geometric structure to the corresponding reduced form. The metal–S distances in the oxidized forms are slightly longer than those in the reduced forms, suggesting a partial oxidation of the metal–S bonds. Electronically, the catalytic metal centre has a more positive charge in the oxidized than that in the reduced species. It is also noted that the Zr centres in **b** and **c** are more positively charged compared with Ti in **a**, in line with the stronger acidity of the former than of the latter. In all cases, the ferrocene iron centres have a lower positive charge than the group 4 metals.

In addition, our DFT calculations indicate that the singly occupied molecular orbitals (SOMO) of the three oxidized active species (**a**[ox], **b**[ox], and **c**[ox]) and the spin densities are mainly localized on the ferrocene fragment (Figs 1 and S1), suggesting that the one-electron oxidation is a ferrocene-based process.
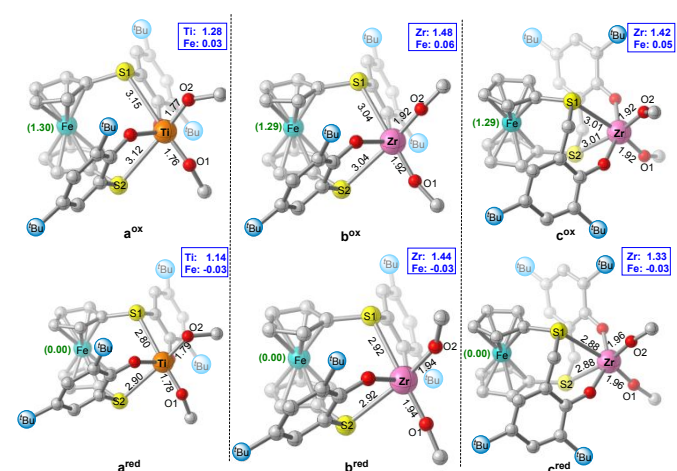

Fig. 1 Optimized structures (distances in Å) of pre-catalysts. All hydrogen atoms were omitted for clarity. The Mulliken charges on metal atoms are given in blue. The data in green given in parenthesis denote the spin density at the iron centers.
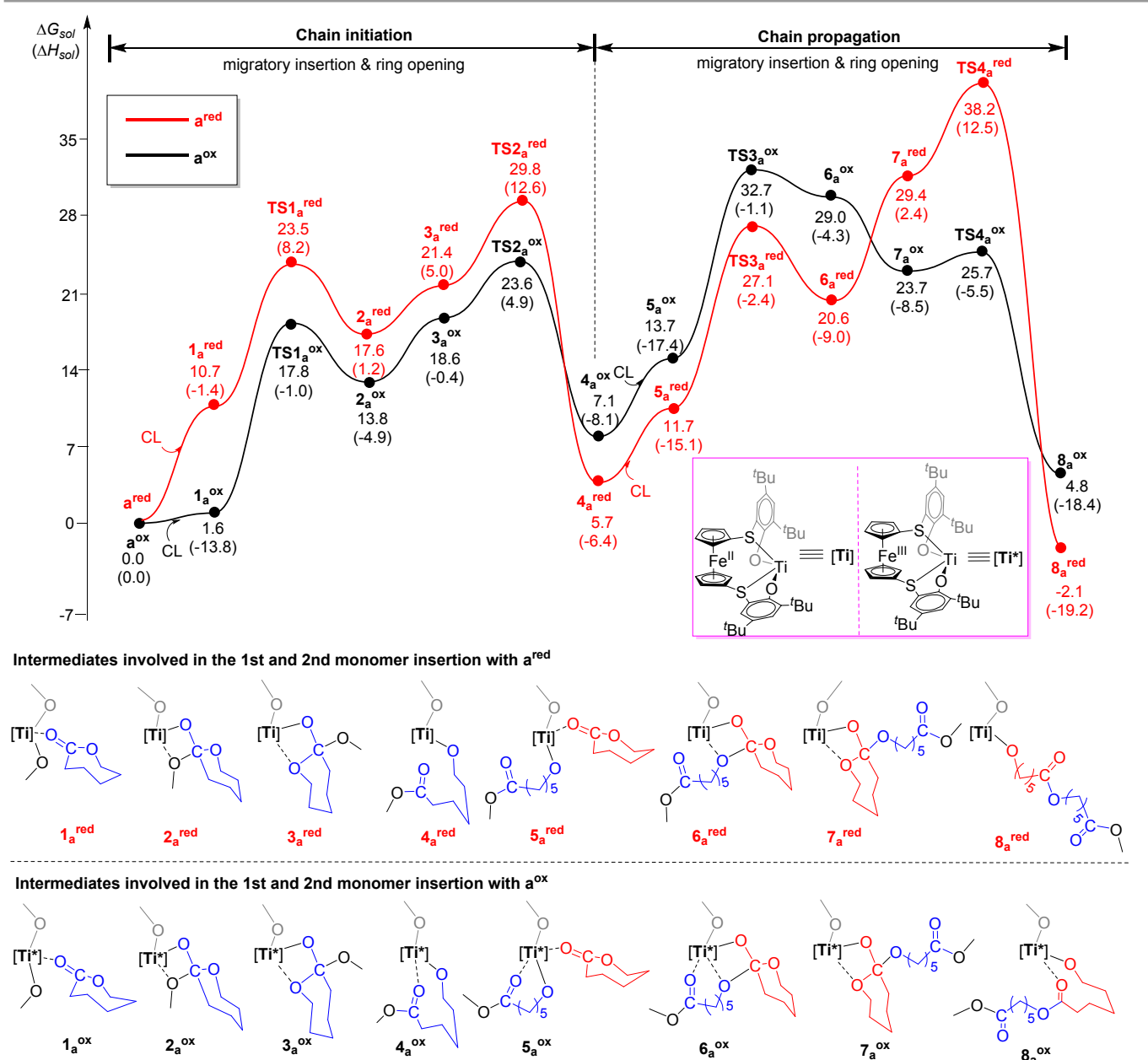
ARTICLE

Fig. 2 Energy profiles of the chain initiation and propagation steps catalyzed by a^{ox} and a^{red}. The relative free energy and enthalpy values (in parentheses) are given in kcal mol^{-1}.

However, we note that the similar one-electron redox process of some ferrocene-containing bi- or multi-nuclear metal complexes did not occur at iron.[20,21] Nonetheless, the results discussed herein still apply.[20]

ROP of CL Catalyzed by a^{ox}/a^{red}

The metal complex catalyzed ROP of cyclic esters such as CL usually follows a coordination-insertion mechanism, which includes a migratory insertion of the alkoxide group and

subsequent ring-opening events.[2d,g,22] Taking this mechanism into account, the chain initiation and propagation steps of CL polymerization catalyzed by **a** (both the oxidized **a**[ox] and reduced **a**[red] species) were calculated. As shown in Fig. 2, the **a**[ox]-catalyzed CL polymerization starts with the formation of **1**[ox]_**a**, which is endergonic by 1.6 kcal mol^{-1}. Then, the migratory insertion of the OMe group into the C=O bond of CL takes place via a transition state (TS), **TS1**[ox]_**a**, with an energy barrier of 17.8 kcal mol^{-1}, leading to the intermediate **2**[ox]_**a**. Prior to ring-opening, an isomerization of **2**[ox]_**a** to **3**[ox]_**a** occurs, during which the Ti···OMe interaction disappears and a new bonding interaction is formed instead between titanium and the ring oxygen atom of the CL unit. Attempts to locate such an isomerization TS were fruitless. However, a relaxed potential energy surface scan indicated that an electronic energy of 7.7 kcal mol^{-1} seems to be required to achieve the isomerization of **2**[ox]_**a** to **3**[ox]_**a** (Fig. S2). Such an energy is lower than that for the ring-opening TS (electronic energy of 7.7 vs 12.3 kcal mol^{-1} relative to **2**[ox]_**a**). Similar results were found for the reduced case (4.2 vs 14.4 kcal mol^{-1} for the electronic versus the activation energy, respectively). These data suggest that such an isomerization event could not be turnover limiting. The subsequent ring-opening goes through the transition state **TS2**[ox]_**a** with an energy barrier of 23.6 kcal mol^{-1}, which is 5.8 kcal mol^{-1} higher than that for the migratory insertion step (**TS1**[ox]_**a**). The resulting ring-opening product **4**[ox]_**a** shows a strong chelation interaction between the carbonyl oxygen and the catalytic center ($d_{\text{Ti-O3}}$ = 2.37 Å, Fig. 3). The whole process of the ring-opening of the first CL is endergonic by 7.1 kcal mol^{-1}.

At the chain propagation stage, similarly to during chain initiation, the carbonyl oxygen of CL coordinates to the Ti center in **4**[ox]_**a**, forming **5**[ox]_**a**. The intermediate **5**[ox]_**a** has a higher free energy than **1**[ox]_**a** by 12.1 kcal mol^{-1} possibly due to a relatively coordinative saturation in the former. The subsequent migratory insertion needs to overcome a high energy barrier of 32.7 kcal mol^{-1} through **TS3**[ox]_**a**, yielding the intermediate **6**[ox]_**a** and, further, **7**[ox]_**a** via isomerization. The subsequent ring opening easily takes place through **TS4**[ox]_**a** to give the product **8**[ox]_**a**. Taken together, the CL polymerization catalyzed by **a**[ox] has an overall activation barrier of 32.7 kcal mol^{-1}, which could be kinetically accessible under the experimental conditions (100

°C). We note that although the reaction is endergonic for the first CL monomer ring opening, the reaction with the second CL implantation is actually exergonic by 2.3 kcal mol^{-1} (the energy of **8**[ox]_**a** relative to **4**[ox]_**a**). In this sense, it would eventually be an exergonic process with the growth of the polymer chain.

In the case of the reduced form **a**[red], the CL polymerization goes through a similar pathway as the oxidized species (Fig. 2). Notably, in **4**[red]_**a** and **8**[red]_**a**, there is no additional Ti···O chelation interaction between Ti and the carbonyl in the pre-enchained CL unit, in contrast to the corresponding oxidized species **4**[ox]_**a** and **8**[ox]_**a** (Fig. 3). In addition, it was found that the ring-opening step of the second CL via **TS4**[red]_**a** has a higher energy barrier (38.2 kcal mol^{-1}) than that for migratory insertion via **TS3**[red]_**a** (27.1 kcal mol^{-1}) and thus serves as the turnover-limiting step of the polymerization catalyzed by the reduced species. Such a high energy barrier makes the reduced form **a**[red] unable to promote the chain propagation, in line with the experimentally observed difference between **a**[ox] and **a**[red].[6f]

It is important to note that, at the chain initiation stage, the reduced species **a**[red] is less active than **a**[ox], as suggested by the corresponding energy barriers (38.2 versus 32.7 kcal mol^{-1} overall activation barrier, Fig. 2). In order to understand this difference further, a distortion/interaction analysis[23] was performed for the transition structures **TS1**[ox]_**a** and **TS1**[red]_**a**. This analysis requires each structure to be divided into two fragments (Fig. 4): the monomer moiety (fragment **B**) and the remaining part (fragment **A**). The energies of these two fragments in the transition state geometry were evaluated through single-point calculations. The single-point energies of the fragments and the energy of the transition state were then used to estimate the interaction energy (ΔE_{int}) between the two fragments. The deformation energy of a fragment is defined as the energy difference between its distorted geometry in the transition state and its optimized structure. Therefore, these single-point energies, together with the energies of the respective fragments in their optimal geometry, allow the estimation of the deformation energies of the two fragments, $\Delta E_{\text{def}}(A)$ and $\Delta E_{\text{def}}(B)$, respectively. As the energy of the transition state, ΔE_{TS}, is evaluated with respect to the energy of the two separated fragments, the relation $\Delta E_{\text{TS}} = \Delta E_{\text{int}} + \Delta E_{\text{def}}(A) + \Delta E_{\text{def}}(B)$ holds.
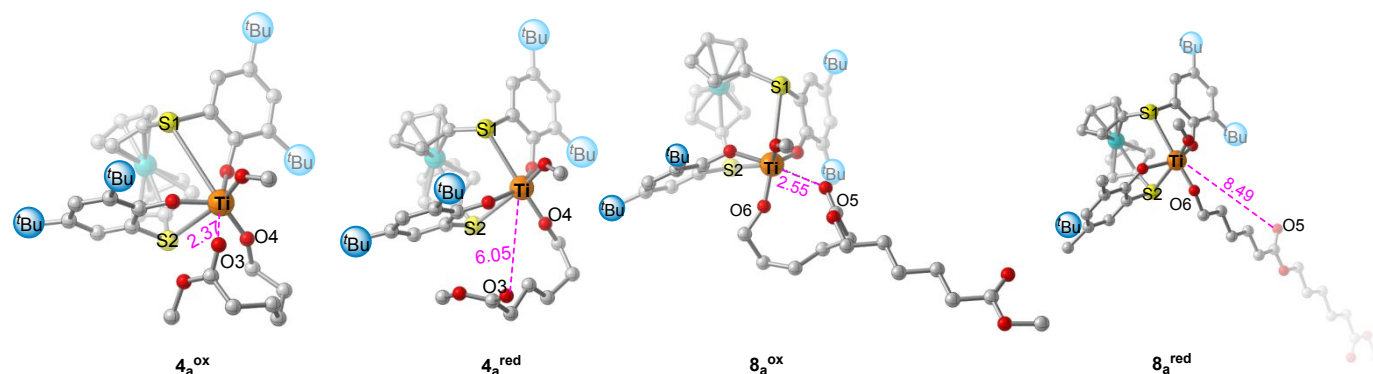

Fig. 3 Optimized structures (distances in Å) of the insertion and ring-opening products of the first and second monomers for the reaction of CL with **a**[ox] and **a**[red].
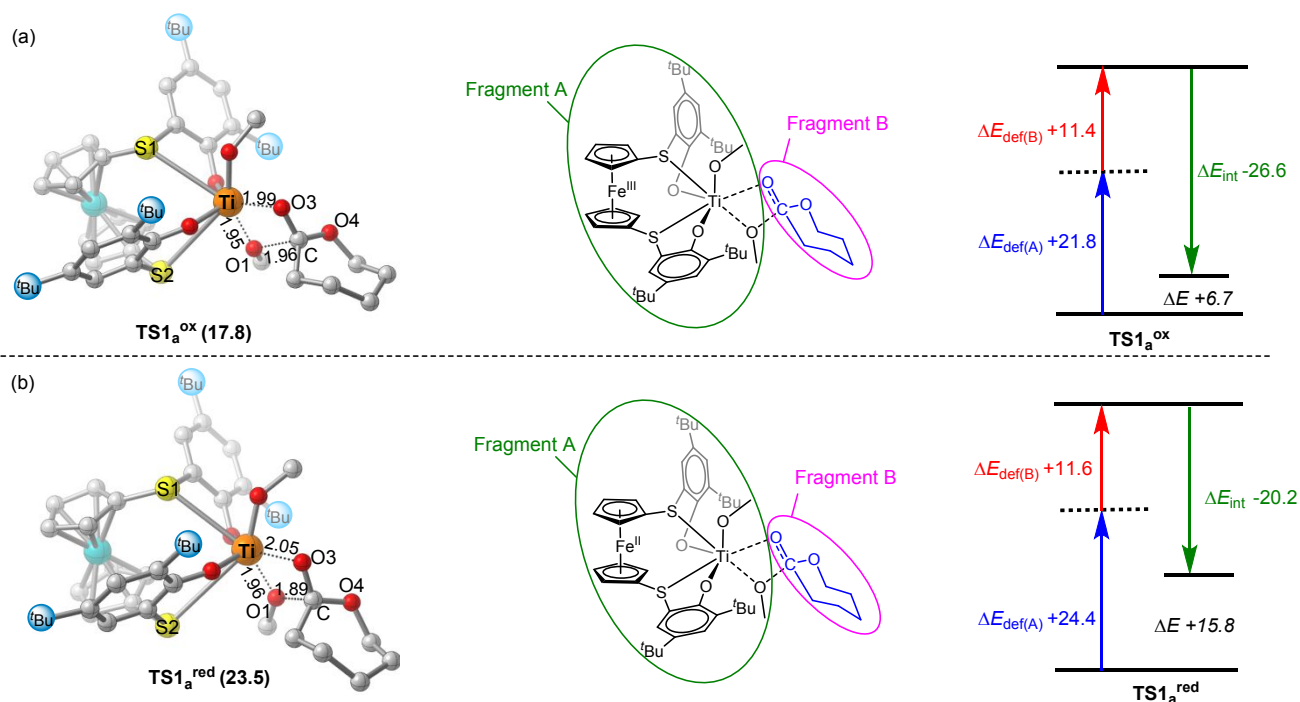
Fig. 4 Optimized structures (distances in Å) and distortion/interaction analysis of **TS1$_a^{ox}$** and **TS1$_a^{red}$**. Values in parentheses are the relative Gibbs free energy barriers. Energies are given in kcal mol^{-1}.

As shown in Fig. 4, the interaction energy ΔE_{int} between the fragments **A** and **B** in **TS1$_a^{ox}$** is significantly more negative than that in **TS1$_a^{red}$** (−26.6 vs −20.2 kcal mol^{-1}). Meanwhile, the total deformation energy ΔE_{def} in **TS1$_a^{ox}$** is also smaller than that in **TS1$_a^{red}$** (11.4 + 21.8 = 33.2 vs 11.6 + 24.4 = 36.0 kcal mol^{-1}). Overall, the ΔE_{TS} value of **TS1$_a^{ox}$** is smaller than that of **TS1$_a^{red}$** (6.7 vs 15.8 kcal mol^{-1}). Therefore, both the stronger interaction (more negative interaction energy) between the two fragments and the less deformation account for the lower energy of **TS1$_a^{ox}$** in comparison with **TS1$_a^{red}$**, with the interaction between the two fragments being dominant. It is noteworthy that, during the chain propagation, the intermediates **4$_a$**, **5$_a$**, and **6$_a$** in their oxidized forms have higher relative free energies than the corresponding reduced species (Fig. 2). This phenomenon is different from that in the chain initiation. This is possibly due to different enthalpy effects as suggested by the corresponding enthalpy values (Fig. 2), where the oxidized forms of **4$_a$**, **5$_a$**, and **6$_a$** are lower in enthalpy compared with their reduced forms, being similar to that in the chain initiation step. As to the higher relative free energy of **TS3$_a^{ox}$** than of **TS3$_a^{red}$**, it is possible that the coordination of the carbonyl of the pre-enchained CL unit makes titanium more crowded; in turn, this weakens the interaction between titanium and an incoming CL monomer and further destabilizes **TS3$_a^{ox}$** (Fig. S3). This is different from what was observed for the aluminum complex supported by the same ligand,[6b] where the propagation step was facilitated by the chelation effect in the oxidized state.

As mentioned above, the ring-opening step of the propagation stage, **TS4$_a^{red}$** has a significantly higher relative energy than **TS4$_a^{ox}$** (38.2 vs 25.7 kcal mol^{-1}, Fig. 2). A closer analysis of the structures of these two transition states could

provide further information to understand such an energy difference. As shown in Fig. 5, the Ti-O6 and Ti-O5 distances in **TS4$_a^{ox}$** are shorter than the corresponding values in **TS4$_a^{red}$** (2.01 vs 2.09 Å, 1.96 vs 1.97 Å, respectively), suggesting a stronger interaction between titanium and the growing chain in the oxidized species. This result is similar to that observed for the initiation step (**TS2$_a^{ox}$** and **TS2$_a^{red}$**, Fig. 5). Therefore, the stronger interaction between the metal center and the growing chain (or incoming monomer) is likely responsible for the higher reactivity of the oxidized than the reduced species, as experimentally observed. Such a stronger interaction in the oxidized forms could be reasonably attributed to the stronger Lewis acidity of the titanium center, as manifested by the higher positive charges in comparison with those of the reduced forms (Fig. S4). This situation is different from the redox-switchable polymerization of trimethylene carbonate by an indium complex, where the ferrocene-oxidation induced elongation of In–N distances rather than the Lewis acidity of the metal center allowed a stronger monomer binding.[9]

ROP of CL Catalyzed by b^{ox}/b^{red}

As aforementioned, the Zr complexes **b^{ox}** and **b^{red}** showed a dramatically different activity compared with their Ti analogues (**a^{ox}/a^{red}**).[6a,f] Unlike **a^{ox}/a^{red}**, **1$_b^{red}$** was more active than **1$_b^{ox}$** toward CL polymerization.[6a] To have a better understanding of such an experimental observation, the energy profiles of CL polymerization mediated by **b^{ox}** and **b^{red}** were investigated. As shown in Fig. 6, the initial monomer coordination in **1$_b^{ox}$** is more stable than the isolated **b^{ox}** and CL monomer by 5.5 kcal mol^{-1}, while its reduced analogue **1$_b^{red}$** is higher in energy than the

reactants by 5.6 kcal mol^{-1}. In the case of the oxidized species, 1_b^{ox} subsequently undergoes the migratory insertion ($TS1_b^{ox}$) and ring opening ($TS2_b^{ox}$) by overcoming energy barriers of 17.8 (5.5 + 12.3) and 20.7 (5.5 + 15.2) kcal mol^{-1}, respectively, yielding the intermediate 4_b^{ox} with a carbonyl chelation interaction ($d_{(Zr\cdots O3)}$ = 2.34 Å, Fig. S5). During chain propagation, the coordination of CL to 4_b^{ox} is exergonic by 4.3 kcal mol^{-1}, similar to the chain initiation step. Then, a migratory insertion occurs via $TS3_b^{ox}$ with an energy barrier of 23.0 kcal mol^{-1} (1_b^{ox} →$TS3_b^{ox}$), yielding 6_b^{ox}. After an isomerization of 6_b^{ox} to 7_b^{ox}, the ring opening reaction takes place to give the product 8_b^{ox}. The overall free energy barrier of the 1_b^{ox}-catalyzed pathway is 28.7 (5.5 + 23.2) kcal mol^{-1} ($TS4_b^{ox}$) relative to 1_b^{ox}. In the case of the reduced species, although the stationary points are higher in

energy than those for the corresponding oxidized species, the overall energy barrier is only 25.1 kcal mol^{-1} ($TS4_b^{red}$), which is lower than that for the reaction profile involving the oxidized species (28.7 kcal mol^{-1}) according to the energy span model.[24] This result suggests that the activity of b^{red} is higher than that of b^{ox}, in agreement with the experimentally observed reactivity difference between the two oxidation states.[6a] A comparison of the two pathways (Fig. 6) indicates that the higher energy barrier for the oxidized species is caused by the higher stability of 1_b^{ox} and 5_b^{ox} than of b^{ox}. In view of the shorter Zr···O(carbonyl) distance in 1_b^{ox} than in 1_b^{red} (2.33 vs 2.40 Å, Fig. S6), this stability may be originated from a stronger binding between the metal center and the coordinating monomer. To verify this hypothesis,
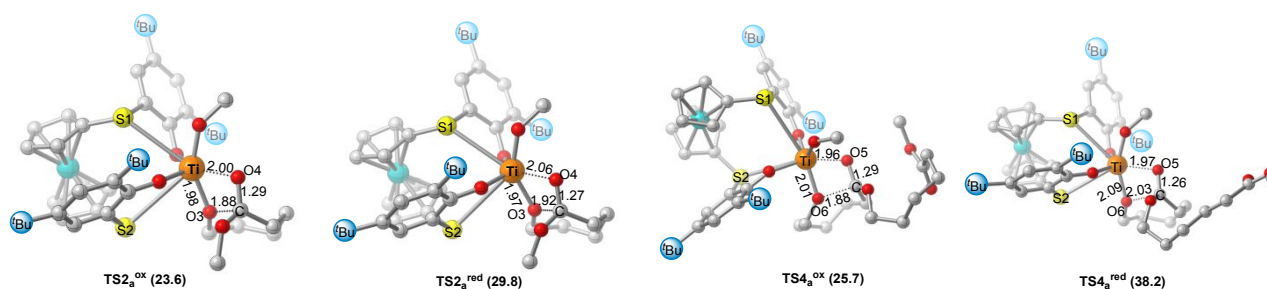

Fig. 5 Optimized structures (distances in Å) and energies of the transition states ($TS2_a^{ox}$ *vs* $TS2_a^{red}$, $TS4_a^{ox}$ *vs* $TS4_a^{red}$). Values in parentheses are the free energies relative to isolated reactants. Energies are given in kcal mol^{-1}.

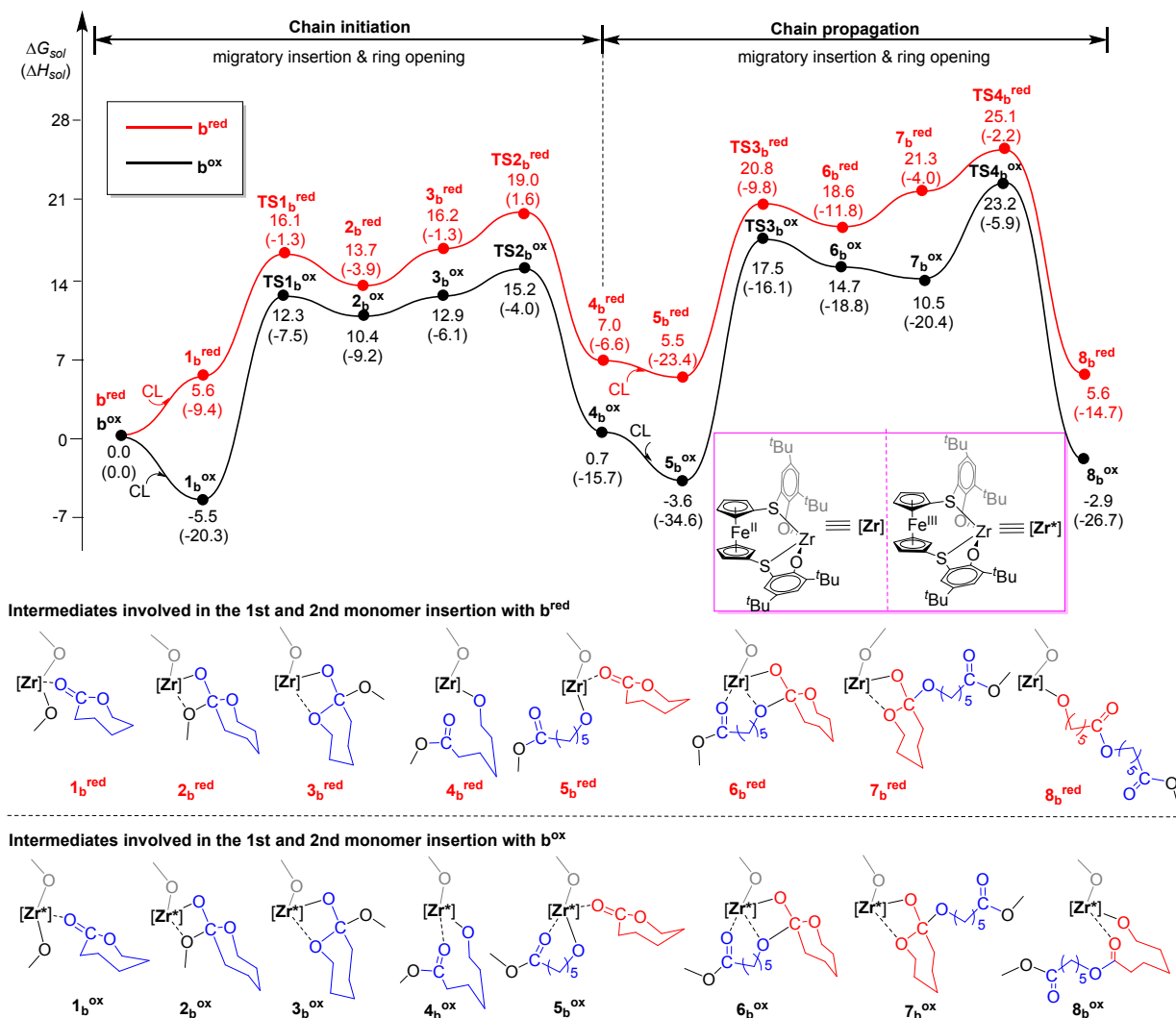**Fig. 6** Energy profiles of the chain initiation and propagation steps catalyzed by b^{ox} and b^{red}. The relative free energy and enthalpy values (in parentheses) are given in kcal mol^{-1}.

the binding energies (ΔE_{bind}) between the CL monomer moiety and the remaining part in $1_b{}^{ox}$ and $1_b{}^{red}$ were calculated. The coordination complex $1_b{}^{ox}$ or $1_b{}^{red}$ can be divided into two fragments, the CL moiety and the remaining part. ΔE_{bind} is defined as the difference between the energy of whole compound and the energy sum of the two fragments. As expected, the results show that the binding in $1_b{}^{ox}$ is stronger than that in $1_b{}^{red}$ (ΔE_{bind} values of −19.9 vs −13.3 kcal mol^{-1}). The difference in the binding energy could be ascribed to the charge and thus the Lewis acidity of the catalytic metal center. For example, the Mulliken charge of Zr in $1_b{}^{ox}$ is more positive compared to that in $1_b{}^{red}$ (1.60 vs 1.40), and the similar is true for $5_b{}^{ox}$ and $5_b{}^{red}$ (see also the detailed change in the catalytic metal center charge along with the reaction pathway shown in Fig. S7).

In comparison with the a^{red}/a^{ox} system, the energy barriers for the **b**-mediated reactions are lower (28.7 and 25.1 vs 32.7 and 38.2 kcal mol^{-1}, Figs 2 and 6), suggesting an overall higher activity of catalysts **b** than **a**. This is in line with the experimental findings that the CL conversion in the b^{red}/b^{ox} system (50 °C) is higher than that in the a^{red}/a^{ox} systems (100 °C).[6a,f] This could

be attributed to the stronger interaction between the active species and monomers in the b^{red}/b^{ox} systems, a consequence of the stronger Lewis acidity of the catalytic metal center in b^{red}/b^{ox}, as suggested by its charge (1.44 in b^{red} vs 1.14 in a^{red}, 1.48 in b^{ox} vs 1.28 in a^{ox}, Fig. 1).

ROP of CL Catalyzed by c^{ox}/c^{red}

Compared with b^{ox}/b^{red} system, the supporting ligand in c^{ox}/c^{red} has an additional methylene unit linking sulphur and the phenyl group. This difference renders **c** with a different redox switchable property.[6a,f] That is, unlike **b**, c^{ox} was more active than c^{red} toward CL polymerization.[6f] This phenomenon stimulated us to study the c^{ox}/c^{red} mediated CL ROP. As shown in Fig. 7, all of the stationary points involved in the c^{ox}-mediated reaction pathway are more stable than those of the corresponding reduced species. The overall energy barriers are 26.2 (4.0 + 22.2) kcal mol^{-1} ($TS4_c{}^{ox}$) and 31.3 kcal mol^{-1} ($TS4_c{}^{red}$) for the oxidized and reduced cases, respectively. This result is in line with the experimentally observed difference between the two states.[6f] The distortion/interaction (Fig. S8) and geometric structure (Figs. S9 and S10) analyses show that the stronger

interaction between the catalyst and the monomer moieties contribute to the higher stability of the oxidized species. This can be also attributed to the relatively stronger Lewis acidity of the catalytic metal center in the oxidized species (Fig. S11) that could be responsible for the switchable activity, similarly to the aforementioned systems **a**[red]/**a**[ox] and **b**[red]/**b**[ox].

The Wiberg bond indices (WBI) of the Zr–S and Zr–O (ancillary ligand) bonds in **b**[ox]/**b**[red] are larger than those in **c**[red]/**c**[ox] (Table S1), suggesting a stronger Zr–ligand binding. This could provide an explanation for the more positively charged Zr atom in **b** than in **c** (Fig. 1).

Effects of Metal Centre and Auxiliary Ligand

According to the discussion above, it is noteworthy that the Lewis acidity of the metal center and the chelation of the lactone carbonyl group play an important role in the redox-switchable activity of the group 4 metal complexes toward ROP of CL. In order to understand trends in these redox-switchable systems, analogous species with different catalytic metal centers and donors in the supporting ligand were modeled computationally. For example, replacing the catalytic metal Zr with Hf gives **d**[ox]/**d**[red], and replacing the coordinating S atom by O and Se atoms, provides **e**[ox]/**e**[red] and **f**[ox]/**f**[red], respectively (Fig. 8). It was found that the Lewis acidity of the catalytic metal centers is different between the two states of the newly designed species except for **e**, where both species show the same charge for zirconium (Fig. 8). Interestingly, species **e** show the highest zirconium charge (1.61) of all the investigated species. The chain initiation and propagation of CL polymerization catalyzed by **d**[ox]/**d**[red], **e**[ox]/**e**[red], and **f**[ox]/**f**[red] were also calculated and the relevant data are collected in Table 2. The corresponding data of **a**[ox]/**a**[red], **b**[ox]/**b**[red], and **c**[ox]/**c**[red] systems are also included in this table for comparison. The results suggest that **d**[ox]/**d**[red] and **f**[ox]/**f**[red] have a similar catalytic performance, as suggested by the energy barriers (31.5 kcal mol^{-1} for both oxidized forms, 24.3 and 24.7 kcal mol^{-1} for the reduced forms, respectively). In view of the moderate energy barriers for the reduced forms, it seems that both **d**[red] and **f**[red] could achieve ROP of CL under ambient conditions. It is noteworthy that, in comparison with **b**[ox]/**b**[red], **d**[ox]/**d**[red] (or **f**[ox]/**f**[red]) may have a larger activity difference between the two states for the ROP of CL because of their larger energy barrier difference (Table 2). In the case of **e**[ox]/**e**[red], however, the energy barriers are almost same (27.0 and 27.4 kcal mol^{-1}) for the two oxidation states. This suggests that **e** may have no redox-switchable character in the ROP of CL. These results indicate that a careful regulation of the catalytic metal center and the ancillary ligand could provide a different redox-switchable activity toward the ROP of CL.
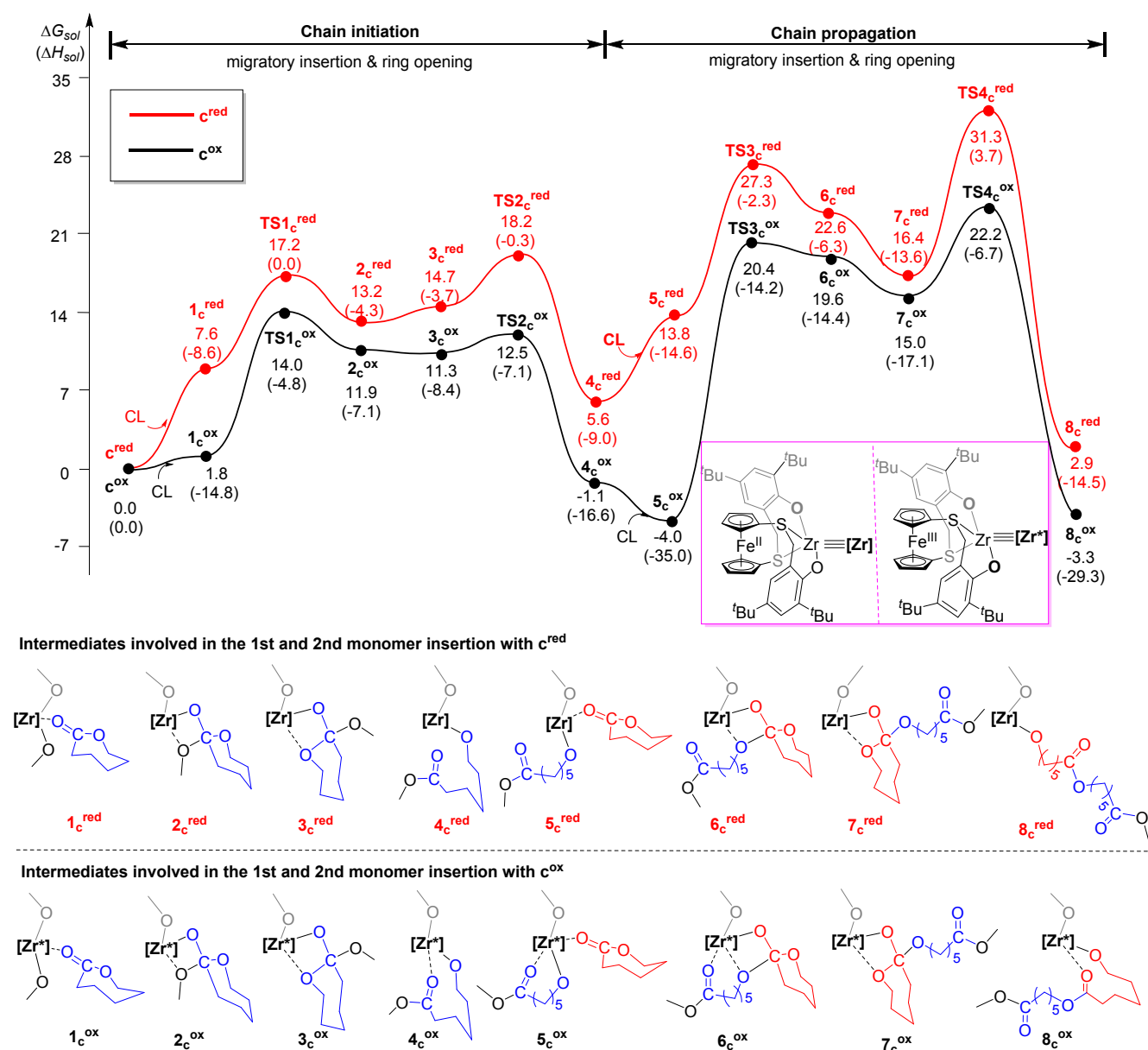
Fig. 7 Energy profiles of the chain initiation and propagation mediated by **c^{ox}** and **c^{red}**. The relative free energies and enthalpy values (in parentheses) are given in kcal mol^{-1}.
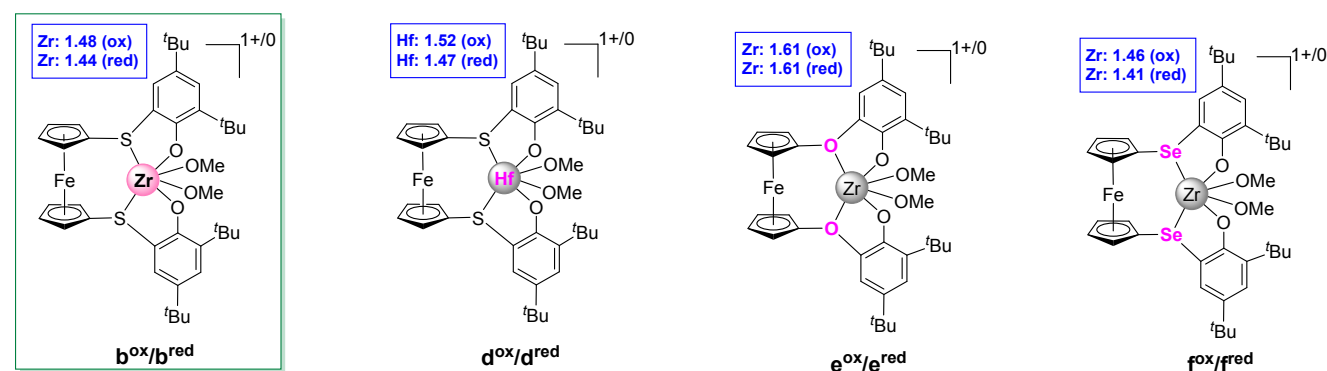

Fig. 8 Designed group 4 metal alkoxide analogues based on the **b^{ox}/b^{red}**. Mulliken charges on metal atoms are given in blue, respectively. The "red" and "ox" in parentheses refer to the reduced and oxidized forms, respectively.

ARTICLE

Table 2. The computed free energies (kcal mol^{-1}) in solution for the chain initiation and propagation of CL polymerization catalyzed by **a-f**.

species	1^a	TS1	TS2	5	TS3	TS4	$\Delta G^{\ddagger\, b}$
a^{ox}	1.6	17.8	23.6	13.7	32.7	25.7	32.7
a^{red}	10.7	23.5	29.8	11.7	27.1	38.2	38.2
b^{ox}	−5.5	12.3	15.2	−3.6	17.5	23.2	28.7
b^{red}	5.6	16.1	19.0	5.5	20.8	25.1	25.1
c^{ox}	1.8	14.0	12.5	−4.0	20.4	22.2	26.2
c^{red}	7.6	17.2	18.2	5.6	27.3	31.3	31.3
d^{ox}	−8.4	10.1	12.4	−2.6	13.4	23.1	31.5
d^{red}	2.3	14.4	17.6	5.3	19.9	24.3	24.3
e^{ox}	−8.5	10.0	11.7	−4.9	10.9	18.5	27.0
e^{red}	6.0	13.3	14.3	7.8	20.4	27.4	27.4
f^{ox}	−3.3	13.2	16.4	0.5	20.9	28.2	31.5
f^{red}	4.8	15.3	18.9	4.7	20.7	24.7	24.7

^{a} **1** and **5** denote the coordination complexes of the first and the second monomer, respectively.
$^b\Delta G^{\ddagger}$ represents the overall free energy barrier for CL polymerization.

Conclusions

The redox-switchable ring-opening polymerization mechanism of ε-caprolactone catalyzed by three group 4 metal complexes bearing [OSSO]-type bis(phenolato) ferrocene ligands (i.e., **a^{ox}/a^{red}**, **b^{ox}/b^{red}**, and **c^{ox}/c^{red}**) was investigated by DFT calculations. Having achieved an agreement between calculation and experiment, it was found that the higher activity of the oxidized forms **a^{ox}** and **c^{ox}** compared to that of their corresponding reduced forms stems from the higher Lewis acidity of the catalytic metal center in the oxidized species. In contrast, the lower activity of the oxidized species **b^{ox}** compared to that of **b^{red}** is due to an increased stability of the intermediate following the monomer coordination that results in a high energy barrier. The current results also indicate that the stronger Lewis acidity of the catalytic metal center generally increases the activity of the catalyst. However, it could also increase the energy barrier of a reaction when the Lewis acidity of metal center is strong enough to overstabilize the coordination complex. It is noteworthy that such a redox-induced Lewis acidity variation and thus switchable activity is different from the case of redox-switchable polymerization of trimethylene carbonate catalyzed by ferrocene-based indium complexes, where the oxidation of the ferrocene unit altered the coordination ability of the catalytic metal center rather than its Lewis acidity. In the series of [OSSO]-type bis(phenolato) ferrocene-based group 4 metal complexes, our computational modelling indicates that a Hf analogue may possess better redox-switchable property for the ROP of CL compared to its corresponding Zr complex. Furthermore, the redox-switchable activity of the Zr complexes with different bridging-heteroatoms in their ancillary ligands follows the order of O < S < Se. These findings are expected to provide useful information on developing new redox-switchable polymerization catalysts for the synthesis of biodegradable polymers from biomass-derived monomers.

Conflicts of interest
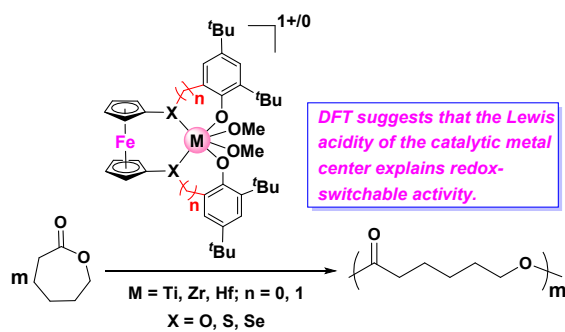
There are no conflicts to declare.

Acknowledgements

Notes and references

1   (a) N. Siddiqui, S. Asawa, B. Birru, R. Baadhe and S. Rao, PCL-based composite scaffold matrices for tissue engineering applications, *Mol Biotechnol*, 2018, **60**, 506; (b) E. Malikmammadov, T. E. Tanir, A. Kiziltay, V. Hasirci and N. Hasirci, PCL and PCL-based materials in biomedical applications, *J. Biomater. Sci., Polym. Ed.* 2018, **29**, 863; (c) R. Auras, L. -T. Lim, S. E. M. Selke and H. Tsuji, Poly(*lactic acid*): *synthesis, structures, properties, processing, and applications*, 2010, Wiley & Sons, Inc.

2   (a) K. M. Osten and P. Mehrkhodavandi, Indium catalysts for ring opening polymerization: exploring the importance of

catalyst aggregation, *Acc. Chem. Res.* 2017, **50**, 2861; (b) T. Fuoco and D. Pappalardo, Aluminum alkyl complexes bearing salicylaldiminato Ligands: versatile initiators in the ring-opening polymerization of cyclic esters, *Catalysts* 2017, **7**, 64; (c) S. Dagorne, M. Normand, E. Kirillov and J.-F. Carpentier, Gallium and indium complexes for ring-opening polymerization of cyclic ethers, esters and carbonates, *Coord. Chem. Rev.* 2013, **257**, 1869; (d) S. Dutta, W. -C. Hung, B.-H. Huang and C.-C. Lin, Recent developments in metal-catalyzed ring-opening polymerization of lactides and glycolides: preparation of polylactides, polyglycolide, and poly(lactide-co-glycolide), *Adv. Polym. Sci.* 2012, **245**, 219; (e) M. Labet and W. Thielemans, Synthesis of polycaprolactone: a review, *Chem. Soc. Rev.* 2009, **38**, 3484; (f) J. Wu, T. Yu, C. Chen and C. Lin, Recent developments in main group metal complexes catalyzed/initiated polymerization of lactides and related cyclic esters, *Coord. Chem. Rev.* 2006, **250**, 602; (g) O. Dechy-Cabaret, B. Martin-Vaca, D. Bourissou, Controlled ring-opening polymerization of lactide and glycolide, *Chem. Rev.* 2004, **104**, 6147; (h) B. J. O'Keefe, M. A. Hillmyer and W. B. Tolman, Polymerization of lactide and related cyclic esters by discrete metal complexes, *J. Chem. Soc., Dalton Trans.* 2001, 2215.

3   (a) J. Wei and P. L. Diaconescu, Redox-switchable ring-opening polymerization with ferrocene derivatives, *Acc. Chem. Res.* 2019, **52**, 415; (b) C. Chen, Redox-controlled polymerization and copolymerization, *ACS Catal.* 2018, **8**, 5506; (c) A. J. Teator, D. N. Lastovickova and C. W. Bielawski, Switchable polymerization catalysts, *Chem. Rev.* 2016, **116**, 1969; (d) S. M. Guillaume, E. Kirillov, Y. Sarazin and J. -F. Carpentier, Beyond stereoselectivity, switchable catalysis: some of the last frontier challenges in ring-opening polymerization of cyclic esters, *Chem. -Eur. J.* 2015, **21**, 7988.

4   C. K. A. Gregson, V. C. Gibson, N. J. Long, E. L. Marshall, P. J. Oxford and A. J. P. White, Redox control within single-site polymerization catalysts, *J. Am. Chem. Soc.* 2006, **128**, 7410.

5   (a) K. R. Delle Chiaie, A. B. Biernesser, M. A. Ortuno, B. Dereli, D. A. Iovan, M. J. T. Wilding, B. Li, C. J. Cramer and J. A. Byers, The role of ligand redox non-innocence in ring-opening polymerization reactions catalysed by bis (imino) pyridine iron alkoxide complexes, *Dalton Trans.* 2017, **46**, 12971. (b) A. B. Biernesser, K. R. Delle Chiaie, J. B. Curley and J. A. Byers, Block copolymerization of lactide and an epoxide facilitated by a redox switchable iron-based catalyst, *Angew. Chem., Int. Ed.* 2016, **55**, 5251; (c) Y. Y. Fang, W. J. Gong, X. J. Shang, H. X. Li, J. Gao and J. P. Lang, Synthesis and structure of a ferric complex of 2, 6-di (1 H-pyrazol-3-yl) pyridine and its excellent performance in the redox-controlled living ring-opening polymerization of ε-caprolactone, *Dalton Trans.* 2014, **43**, 8282; (d) A. B. Biernesser, B. Li and J. A. Byers, Redox-controlled polymerization of lactide catalyzed by bis (imino) pyridine iron bis (alkoxide) complexes, *J. Am. Chem. Soc.* 2013, **135**, 16553; (e) A. Sauer, J. -C. Buffet, T. P. Spaniol, H. Nagae, K. Mashima and J. Okuda, Switching the lactide polymerization activity of a cerium complex by redox reactions, *ChemCatChem* 2013, **5**, 1088; (f) E. M. Broderick, N. Guo, T. Wu, C. S. Vogel, C. Xu, J. Sutter, J. T. Miller, K. Meyer, T. Cantat and P. L. Diaconescu, Redox control of a polymerization catalyst by changing the oxidation state of the metal center, *Chem. Commun.* 2011, **47**, 9897.

6   (a) M. Y. Lowe, S. Shu, S. M. Quan and P. L. Diaconescu, Investigation of redox switchable titanium and zirconium catalysts for the ring opening polymerization of cyclic esters and epoxides, *Inorg. Chem. Front.* 2017, **4**, 1798; (b) J. Wei, M. N. Riffel and P. L. Diaconescu, Redox control of aluminum ring-opening polymerization: a combined experimental and DFT investigation, *Macromolecules* 2017, **50**, 1847; (c) S. M. Quan, J. Wei and P. L. Diaconescu, Mechanistic studies of redox-switchable copolymerization of lactide and cyclohexene oxide by a zirconium complex, *Organometallics* 2017, **36**, 4451; (d) S. M. Quan, X. Wang, R. Zhang and P. L. Diaconescu, Redox switchable copolymerization of cyclic esters and epoxides by a zirconium complex, *Macromolecules* 2016, **49**, 6768; (e) L. A. Brown, J. L. Rhinehart and B. K. Long, Effects of ferrocenyl proximity and monomer presence during oxidation for the redox-switchable polymerization of *L*-lactide, *ACS Catal.* 2015, **5**, 6057. (f) X. Wang, A. Thevenon, J. L. Brosmer, I. Yu, S. I. Khan, P. Mehrkhodavandi and P. L. Diaconescu, Redox control of group 4 metal ring-opening polymerization activity toward *L*-lactide and ε-caprolactone, *J. Am. Chem. Soc.* 2014, **136**, 11264; (g) A, Lai, Z. C. Hern and P. L. Diaconescu, Switchable ring-opening polymerization by ferrocene supported aluminum complexes, *ChemCatChem* 2019, **11**, 4210.

7   M. A. Ortuño, B. Dereli, K. R. D. Chiaie, A. B. Biernesser, M. Qi and J. A. Byers, C. J. Cramer, The role of alkoxide initiator, spin state, and oxidation state in ring-opening polymerization of ε-caprolactone catalyzed by iron bis(imino)pyridine complexes, *Inorg. Chem.* 2018, **57**, 2064.

8   (a) G. Zhou, X. Kang, X. Wang, Z. Hou and Y. Luo, Theoretical investigations of isoprene polymerization catalyzed by cationic half-sandwich scandium complexes bearing a coordinative side arm, *Organometallics* 2018, **37**, 551; (b) C. Wang, G. Luo, M. Nishiura, G. Song, A. Yamamoto, Y. Luo and Z. Hou, Heteroatom-assisted olefin polymerization by rare-earth metal catalysts, *Sci. Adv.* 2017, **3**, e1701011; (c) X. Hu, X. Kang, G. Zhou, X. Wang, Z. Hou and Y. Luo, DFT studies on isoprene/ethylene copolymerization catalyzed by cationic scandium complexes bearing different ancillary ligands, *Chin. J. Chem.* 2017, **35**, 723; (d) X. Kang, G. Zhou, X. Wang, J. Qu, Z. Hou and Y. Luo, Alkyl effects on the chain initiation efficiency of olefin polymerization by cationic half-sandwich scandium catalysts: a DFT study, *Organometallics* 2016, **35**, 913; (e) G. Luo, Y. Luo, Z. Hou and J. Qu, Intermetallic cooperation in olefin polymerization catalyzed by a binuclear samarocene hydride: a theoretical study, *Organometallics* 2016, **35**, 778; (f) L. Luo, X. Kang, G. Zhou, S. Chen, G. Luo, J. Qu and Y. Luo, Mechanistic insights into regioselective polymerization of 1,3-dienes catalyzed by a bipyridine-ligated iron complex: a DFT study, *Int. J. Quantum Chem.* 2016, **116**, 1274; (g) X. Wang, F. Lin, J. Qu, Z. Hou and Y. Luo, DFT studies on styrene polymerization catalyzed by cationic rare-earth-metal complexes: origin of ligand-dependent activities, *Organometallics* 2016, **35**, 3205; (h) X. Kang, A. Yamamoto, M. Nishiura, Y. Luo and Z. Hou, Computational analyses of the effect of Lewis bases on styrene polymerization catalyzed by cationic scandium half-sandwich complexes, *Organometallics* 2015, **34**, 5540; (i) X. Kang, Y. Luo, G. Zhou, X. Wang, X. Yu, Z. Hou and J. Qu, Theoretical mechanistic studies on the trans-1,4-specific polymerization of isoprene catalyzed by a cationic La–Al binuclear complex, *Macromolecules* 2014, **47**, 4596; (j) X. Kang, Y. Song, Y. Luo, G. Li, Z. Hou and J. Qu, Computational studies on isospecific polymerization of 1-hexene catalyzed by cationic rare earth metal alkyl complex bearing a C₃-Pr-trisox ligand, *Macromolecules* 2012, **45**, 640; (k) Y. Luo, Y. Luo, J. Qu and Z. Hou, QM/MM studies on scandium-catalyzed syndiospecific copolymerization of styrene and ethylene, *Organometallics* 2011, **30**, 2908.

9   X. Xu, G. Luo, A. Mehmood, Y. Zhao, G. Zhou, Z. Hou and Y. Luo, Theoretical mechanistic studies on redox-switchable polymerization of trimethylene carbonate catalyzed by an indium complex bearing a ferrocene-based ligand, *Organometallics* 2018, **37**, 4599.

10 (a) J. P. Perdew, K. Burke and Y. Wang, Generalized gradient approximation for the exchange-correlation hole of a many-electron system, *Phys. Rev. B* 1996, **54**, 16533; (b) A. D. Becke, Density-functional thermochemistry. III. The role of exact

ARTICLE

exchange, *J. Chem. Phys.* 1993, **98**, 5648; (c) J. P. Perdew and Y. Wang, Accurate and simple analytic representation of the electron-gas correlation energy, *Phys. Rev. B: Condens. Matter Mater. Phys*. 1992, **45**, 13244.

11 S. Grimme, J. Antony, S. Ehrlich and H. A. Krieg, A consistent and accurate ab initio parametrization of density functional dispersion correction (DFT-D) for the 94 elements H-Pu, *J. Chem. Phys.* 2010, **132**, 154104.

12 A. Lai, J. Clifton, P. L. Diaconescu and N. Fey, Computational mapping of redox-switchable metal complexes based on ferrocene derivatives, *Chem. Commun*., 2019, **55**, 7021.

13 (a) P. C. Hariharan and J. A. Pople, The influence of polarization functions on molecular orbital hydrogenation energies, *Theor. Chim. Acta* 1973, **28**, 213; (b) W. J. Hehre, R. Ditchfield and J. A. Pople, Self-consistent molecular orbital methods. XII. further extensions of Gaussian-type basis sets for use in molecular orbital studies of organic molecules, *J. Chem. Phys.* 1972, **56**, 2257.

14 (a) W. R. Wadt and P. J. Hay, Ab initio effective core potentials for molecular calculations. potentials for main group elements Na to Bi, *J. Chem. Phys*. 1985, **82**, 284; (b) P. J. Hay and W. R. Wadt, Ab initio effective core potentials for molecular calculations. potentials for the transition metal atoms Sc to Hg, *J. Chem. Phys*. 1985, **82**, 270; (c) P. J. Hay and W. R. Wadt, Ab initio effective core potentials for molecular calculations. potentials for K to Au including the outermost core orbitals, *J. Chem. Phys.* 1985, **82**, 299.

15 Y. Zhao and D. G. Truhlar, The M06 suite of density functionals for main group thermochemistry, thermochemical kinetics, noncovalent interactions, excited states, and transition elements: two new functionals and systematic testing of four M06-class functionals and 12 other functionals, *Theor. Chem. Acc*. 2008, **120**, 215.

16 (a) M. Cossi, N. Rega, G. Scalmani and V. Barone, Energies, structures, and electronic properties of molecules in solution with the C-PCM solvation model, *J. Comput. Chem.* 2003, **24**, 669; (b) V. Barone and M. Cossi, Quantum calculation of molecular energies and energy gradients in solution by a conductor solvent model, *J. Phys. Chem. A* 1998, **102**, 1995.

17 (a) J. M. L. Martin and A. Sundermann, Correlation consistent valence basis sets for use with the Stuttgart-Dresden-Bonn relativistic effective core potentials: the atoms Ga-Kr and In-Xe, *J. Chem. Phys.* 2001, **114**, 3408; (b) M. Dolg, H. Stoll and H. Preuss, Energy-adjusted ab-initio pseudopotentials for the rare earth elements, *J. Chem. Phys.* 1989, **90**, 1730.

18 M. J. Frisch, G. W. Trucks, H. B. Schlegel, G. E. Scuseria, M. A. Robb, J. R. Cheeseman, G. Scalmani, V. Barone, B. Mennucci, G. A. Petersson, H. Nakatsuji, M. Caricato, X. Li, H. P. Hratchian, A. F. Izmaylov, J. Bloino, G. Zheng, J. L. Sonnenberg, M. Hada, M. Ehara, K. Toyota, R. Fukuda, J. Hasegawa, M. Ishida, T. Nakajima, Y. Honda, O. Kitao, H. Nakai, T. Vreven, J. A. Montgomery, J. E. Peralta, F. Ogliaro, M. Bearpark, J. J. Heyd, E. Brothers, K. N. Kudin, V. N. Staroverov, T. Keith, R. Kobayashi, J. Normand, K. Raghavachari, A. Rendell, J. C. Burant, S. S. Iyengar, J. Tomasi, M. Cossi, N. Rega, J. M. Millam, M. Klene, J. E. Knox, J. B. Cross, V. Bakken, C. Adamo, J. Jaramillo, R. Gomperts, R. E. Stratmann, O. Yazyev, A. J. Austin, R. Cammi, C. Pomelli, J. W. Ochterski, R. L. Martin, K. Morokuma, V. G. Zakrzewski, G. A. Voth, P. Salvador, J. J. Dannenberg, S. Dapprich, A. D. Daniels, O. Farkas, J. B. Foresman, J. V. Ortiz, J. Cioslowski and D. J. Fox, *Gaussian 16, Revision B.01*, Gaussian, Inc., Wallingford CT, 2016.

19 Legault, C. Y., Cylview, version 1.0 b. *Université de Sherbrooke* 2009, http://www.cylview.org/.

20 M. Abubekerov, V. Vlcek, J. Wei, M. E. Miehlich, S. M. Quan, K. Meyer, D. Neuhauser and P. L. Diaconescu, Exploring oxidation state-dependent selectivity in polymerization of cyclic esters and carbonates with zinc(II) complexes, *iScience* 2018, **7**, 120.

21 Y. Shen, S. M. Shepard, C. J. Reed and P. L. Diaconescu, Zirconium complexes supported by a ferrocene-based ligand as redox switches for hydroamination reactions, *Chem. Commun.,* 2019, **55**, 5587.

22 C. M. Thomas, Stereocontrolled ring-opening polymerization of cyclic esters: synthesis of new polyester microstructures, *Chem. Soc. Rev.* 2010, **39**, 165; (b) A. Arbaoui and C. Redshaw, Metal catalysts for ε-caprolactone polymerization, *Polym. Chem*. 2010, **1**, 801.

23 (a) K. Kitaura and K. Morokuma, A new energy decomposition scheme for molecular interactions within the Hartree-Fock approximation, *Int. J. Quantum Chem.* 1976, **10**, 325; (b) F. M. Bickelhaupt and K. N. Houk, Analyzing reaction rates with the distortion/interaction-activation strain model, *Angew. Chem., Int. Ed.* 2017, **56**, 10070; (c) F. Liu, Y. Liang, and K. N. Houk, Bioorthogonal cycloadditions: computational analysis with the distortion/interaction model and predictions of reactivities, *Acc. Chem. Res.* 2017, **50**, 2297; (d) I. Fernández and F. M. Bickelhaupt, The activation strain model and molecular orbital theory: understanding and designing chemical reactions, *Chem. Soc. Rev.* 2014, **43**, 4953

24 S. Kozuch, S. Shaik, How to conceptualize catalytic cycles? The energetic span model, *Acc. Chem. Res*. 2011, **44**, 101.

TOC Use Only

DFT suggests that the Lewis acidity of the catalytic metal center explains redox-switchable activity.

M = Ti, Zr, Hf; n = 0, 1
X = O, S, Se

DFT calculations indicate that the Lewis acidity of the catalytic metal center **M** (Ti, Zr, Hf) explains the redox-switchable activity observed for the ring-opening polymerization of ε-caprolactone by ferrocene derived metal complexes.